11 The Kondo Effect

Frithjof B. Anders
Theoretische Physik II
Technische Universität Dortmund

Contents

1 Introduction

Jun Kondo was intrigued [1, 2] by the puzzling experimental observation [3] that the resistance in noble or divalent metals typically shows a minimum at low temperatures when containing small concentrations of transition metals. It was expected that the inelastic scattering is reduced with decreasing temperature and, therefore, the resistance should be a monotonic function of T, which reaches a finite temperature-independent value for $T \to 0$ proportional to the remaining lattice imperfections. It had been noted that the increase of the residual resistance is proportional to the transition metal concentration [3, 4] and only occurs when those impurities are magnetic. In 1961, Anderson [5] proposed a simple model for the understanding of the formation of stable magnetic moments in transition metals ions. Since the Coulomb interactions is only weakly screened on atomic length scales, valence fluctuations on unfilled d and f shells are suppressed at integer fillings, and a finite total angular momentum is formed according to Hund's rules. The Anderson model, which we will discuss in Sec. 1.2, provides a microscopic understanding of the Friedel sum rule [6] which relates the phase shifts of the conduction electrons scattered on the impurity to the number of displaced electrons.

The overwhelming experimental evidence hints towards the generic nature of this effect: the details of the conduction bands actually do only enter into a single material-dependent low energy scale T_K, the so-called Kondo scale. Kondo realized that the position of the resistance minimum remains unaltered when reducing the concentration of the magnetic impurities which rules out interaction induced correlation effects between different localized spins. From the first observation [3] in 1934, it took three decades until Kondo [1, 2] proposed his seminal Hamiltonian, which provides a simple physical picture and explains the experimental data. In the Kondo model,

$$H = H_b + H_K \,, \tag{1}$$

the conduction electrons are described by a non-interacting electron gas

$$H_b \;=\; \sum_{\vec{k}\sigma} \varepsilon_{\vec{k}\sigma} c^\dagger_{\vec{k}\sigma} c_{\vec{k}\sigma} \tag{2}$$

and the interaction with a localized magnetic moment $\vec{S}$ is modelled by a simple Heisenberg term

$$H_K \;=\; J\vec{S}\vec{s}_b \,. \tag{3}$$

$c^\dagger_{\vec{k}\sigma}$ ($c_{\vec{k}\sigma}$) generates (destroys) a conduction electron with momentum $\vec{k}$ and spin σ, $\vec{S}$ represents the impurity spin, $\vec{s}_b$

$$\vec{s}_b = \frac{1}{2}\frac{1}{N} \sum_{\vec{k}\vec{k}'} \sum_{\alpha\beta} c^\dagger_{\vec{k}\alpha}\, \underline{\vec{\sigma}}_{\alpha\beta}\, c_{\vec{k}'\beta} \tag{4}$$

is the spin of the conduction electrons at the impurity site and $\underline{\vec{\sigma}}$ are the Pauli matrices. The lattice has a finite size of N sites which are sent to $N \to \infty$ in the thermodynamic limit.

Over the period of the last 50 years we have learned that the Kondo problem is not restricted to magnetically doped noble or divalent metals: it has turned out to be one of the most fundamental

problems in solid state physics. It involves the change of ground states when going from high-energy to low energy physics indicated by the infrared divergent perturbation theory.

1.1   Resistance minimum

Before we proceed to the Kondo problem itself, let us investigate the scattering of free conduction electrons on a finite number of impurities. The N_{imp} identical impurities are located at positions $\{\vec{R}_i\}$, and each contributes a potential $V(\vec{r} - \vec{R}_i)$ to H_b generating the additional potential scattering term

$$V = \sum_i \sum_{\vec{k}\vec{q}\sigma} e^{i\vec{q}\vec{R}_i} V(\vec{q})\, c^\dagger_{\vec{k}+\vec{q},\sigma} c_{\vec{k}\sigma}\,, \tag{5}$$

where $V(\vec{q})$ is the Fourier transform of $V(\vec{r})$. For a given configuration of impurities, $\{\vec{R}_i\}$, the single-particle Green function of the conduction electrons is determined by Dyson's equation [7],

$$G_{\vec{k},\vec{k}'}(z) = \frac{\delta_{\vec{k},\vec{k}'}}{z - \varepsilon_{\vec{k}\sigma}} + \sum_i \sum_{\vec{q}\sigma} e^{i\vec{q}\vec{R}_i} V(\vec{q})\, G^0_{\vec{k}}(z) G_{\vec{k}-\vec{q},\vec{k}'}(z)\,, \tag{6}$$

where $G^0_{\vec{k}}(z) = [z - \varepsilon_{\vec{k}\sigma}]^{-1}$. After expanding this equation in powers of $V(\vec{q})$, we need to average over the different configurations $\{\vec{R}_i\}$ in order to obtain the configuration averaged Green function $\langle G_{\vec{k},\vec{k}'}(z)\rangle_{\text{conf}}$. In linear order, we obtain

$$\left\langle \sum_i e^{i\vec{q}\vec{R}_i} V(\vec{q}) \right\rangle = N_{imp}V(0)\, \delta_{\vec{q},0}\,, \tag{7}$$

while in second order, two terms [4] arise

$$\left\langle \sum_i e^{i\vec{q}\vec{R}_i} V(\vec{q}) \sum_j e^{i\vec{q'}\vec{R}_j} V(\vec{q'}) \right\rangle = N_{imp}V(q)V(q')\delta_{\vec{q}+\vec{q'},0} + N_{imp}(N_{imp}-1)V^2(0)\delta_{\vec{q},0}\delta_{\vec{q'},0}\,. \tag{8}$$

The first describes two scattering events on a single impurity and the other a single scattering of two different impurities. Summing up all these zero momentum transfers $V(0)$ produces a uniform background which we absorb into the dispersion $\varepsilon_{\vec{k}\sigma}$. In higher order, there are two types of skeleton diagrams [8] generated: either the diagram describes multiple scattering on a single impurity, or several impurities are involved. The latter include interference effects which can be neglected if the mean free path is shorter than the average distance between two impurities. In the following, we assume such a small concentration of c_{imp} that the condition $c_{imp} = N_{imp}/N \ll 1$ is always fulfilled. Then $G_{\vec{k}}(z) = [z - \varepsilon_{\vec{k}\sigma} - \Sigma_{\vec{k}}(z)]^{-1}$ acquires a self-energy

$$\Sigma_{\vec{k}}(z) = c_{imp}T_{\vec{k}}(z), \tag{9}$$

which is proportional to the impurity concentration. The scattering matrix $T_{\vec{k}}(z)$ accounts for the sum of all multi-scattering processes on a single impurity.

The imaginary part of the self-energy is related to the single-particle life-time $\tau_{\vec{k}}$:

$$\Im m \Sigma_{\vec{k}}(\varepsilon_k - i\delta) = 1/2\tau(\vec{k}) \,,$$

whose value close to the Fermi energy might be mistaken for a transport life-time entering the simple Drude model for the conductance,

$$\sigma = \frac{ne^2 \tau_{Drude}}{m} \,, \tag{10}$$

where n is the concentration of electrons. According to Kubo's transport theory [7], however, the conductance is obtained from the current-current correlation function. A closer inspection reveals immediately that this correspondence of single-particle and transport life-time is incorrect in general: Clearly, forward scattering by the T-matrix contributes less to resistance than backward scattering. Hence, the average over the momentum transfer directions is required to connect τ_{Drude} with $T_k(z)$. However, we can employ the optical theorem to connect the imaginary part of the forward scattering $\Im m T_{\vec{k}}(z)$ to the angular integrated matrix elements $\Im m T_k(z) \propto \int d\Omega |\langle \vec{k} | \hat{T} | \vec{k}' \rangle|^2$. Since we deal with isotropic s-wave scattering in the Kondo problem, the T-matrix becomes angular independent and the angular averaging yields $\tau_{Drude} = \tau_{k_F}$.

Just taking the contribution linear in J, the spin-diagonal scattering of conduction electrons reads JS_z and the spin flip terms yields $\langle \vec{k} \uparrow | \hat{T} | \vec{k}' \downarrow \rangle = JS^-$, so that all three contributions from the scalar product $J\vec{S}\vec{s}_b$ add up to $\Im m T = J^2 S(S+1) + O(J^3)$ using the optical theorem. In second order in J, we just find a constant contribution similar to a residual potential scattering term. Its magnitude, however, is proportional to the square of the effective moment.

In order to understand Kondo's theory of the resistance minimum, the second order contribution to the T-matrix [1]

$$\langle \vec{k}\sigma | \hat{T} | \vec{k}'\sigma' \rangle|_{(2)} = \left\langle \vec{k}\sigma \left| H_K \frac{1}{z - \hat{H}_0} H_K \right| \vec{k}'\sigma' \right\rangle \tag{11}$$

is needed. Since the details of the calculation can be found in Hewson's book [4], and a similar calculation is presented in the Sec. 2.1 below, we will only state the final result for the resistivity contribution of a single impurity:

$$\rho_{imp} = \frac{3\pi m J^2 S(S+1)}{2e^2 \hbar \varepsilon_F} \left[1 - J\rho(\varepsilon_F) \ln \left(\frac{k_B T}{D} \right) + O(J^3) \right] \,, \tag{12}$$

where m is the electron mass, $\rho(\varepsilon_F)$ the conduction band density of state at the Fermi energy ε_F and D the band width. The infrared divergent logarithm arises from the integration of the resolvent $1/(z - \hat{H}_0) \propto 1/(z - \varepsilon)$ over all intermediate conduction electron states since the spin-flipped local states are degenerate. In a magnetic field, however, the logarithmic divergency will be cut off on the energy scale given by the Zeeman energy.

Typically, the bare coupling $g = J\rho(\varepsilon_F) \ll 1$ is small. However, the logarithmic corrections causes an increase in ρ_{imp} for decreasing temperatures and $J > 0$, which diverges for $T \to 0$. The effective scattering rate becomes of the order $\mathcal{O}(1)$ at temperatures of an exponentially small energy scale T_K

$$T_K \propto D e^{-\frac{1}{\rho J}} \,, \tag{13}$$

which is non perturbative in the bare coupling constant ρJ. This scale indicates the breakdown of the perturbation theory and is called the Kondo scale. At the heart of the problem are divergent spin-flip contributions, which occur in quantum impurity problems with degenerate local quantum states.

1.2 Anderson model

As mentioned already in the introduction, Anderson proposed a model [5] for the understanding of local moment formation in 1961. Its simplest version comprises of a single localized spin-degenerate level with energy ε^d and a Coulomb repulsion U when the level is filled with two electrons of opposite spin. This local Hamiltonian

$$H_{imp} = \sum_\sigma \varepsilon^d d_\sigma^\dagger d_\sigma + U n_\uparrow n_\downarrow \tag{14}$$

is then trivially diagonalized by the four atomic states $|0\rangle, |\sigma\rangle, |2\rangle$. For the single particle energy we use the notation ε^d which is identical to ε_f in Bulla's lecture. This different notation roots historically in the modeling of either d-electron or f-electron systems.

Such an atomic orbital [5] is then coupled to a single conduction band

$$H_b = \sum_{\vec{k}\sigma} \varepsilon_{\vec{k}\sigma} c_{\vec{k}\sigma}^\dagger c_{\vec{k}\sigma} \tag{15}$$

via a hybridization term

$$H_{mix} = \sum_{\vec{k}\sigma} V_{\vec{k}} \left(c_{\vec{k}\sigma}^\dagger d_\sigma + d_\sigma^\dagger c_{\vec{k}\sigma} \right) . \tag{16}$$

The local dynamics of the single-impurity Anderson model (SIAM), defined by the Hamiltonian

$$H_{SIAM} = H_{imp} + H_b + H_{mix} \tag{17}$$

is completely determined by the hybridization function

$$\Gamma_\sigma(\omega) = \pi \sum_{\vec{k}} |V_{\vec{k}}|^2 \delta(\omega - \varepsilon_{\vec{k}\sigma}) . \tag{18}$$

The SIAM and the Kondo model belong to the class of quantum impurity models (QIM) which are defined by a finite number of local degrees of freedom, which are coupled to one or more bath continua.

In the regime $\varepsilon^d < 0$ and $\varepsilon^d + U > 0$, the energies of the empty and double occupied state, $|0\rangle$ and $|2\rangle$, lie above the $|\sigma\rangle$ states and can be neglected at low temperatures: a local moment represented by a spin $1/2$ is formed. Although local charge fluctuations on the d-level are suppressed at low temperatures and odd integer fillings, virtual exchange of electrons with the conduction are still possible, leading to spin-flip processes. Using a unitary transformation, Schrieffer and Wolff have derived [9] an effective energy dependent Kondo coupling J_{eff} between the local conduction electron and the two local moment states $|\sigma\rangle$. First, the Fock space

is partitioned into a low energy sector, which contains $|\sigma\rangle$, projected out by $\hat{P}_L$ and its complement $\hat{P}_H = (\hat{1} - \hat{P}_L)$ which includes $|0\rangle$ and $|2\rangle$. The Hamiltonian can then be divided into a diagonal part $H_d = \hat{P}_L H \hat{P}_L + \hat{P}_H H \hat{P}_H$ and an off-diagonal part $\lambda V = \hat{P}_L H \hat{P}_H + \hat{P}_H H \hat{P}_L$. The subsequent unitary transformation $U = \exp(\lambda S)$

$$H' = e^{\lambda S} H e^{-\lambda S} = H_d + \frac{\lambda^2}{2}[S, \bar{V}] + \sum_{n=2} \lambda^{n+1} \frac{n}{n+1!}[S, \bar{V}]_n \,, \tag{19}$$

is defined by the requirement of eliminating V in first order. The generator S is determined by the condition $[S, H_d] = -V$. Then, the effective Hamiltonian of the low energy subspace

$$H'_{LL} = \hat{P}_L H' \hat{P}_L = \hat{P}_L H \hat{P}_L + P_L \frac{\lambda^2}{2}[S, \bar{V}] P_L + O(\lambda^3) \tag{20}$$

acquires renormalized parameters and additional interaction terms via virtual transitions between the low and the high energy sectors mediated by V up to second order in λ. By applying this transformation to the H_{SIAM}, $H_K = \hat{P}_L \frac{\lambda^2}{2}[S, \bar{V}]\hat{P}_L$ takes the form of the Kondo interaction [9]

$$\begin{aligned} H_K &= \frac{1}{2} \sum_{\vec{k},\vec{k}'} \sum_{\alpha\beta} J_{\vec{k}\vec{k}'} c^{\dagger}_{\vec{k}\alpha} \vec{\sigma}_{\alpha\beta} c_{\vec{k}'\beta} \vec{S} \\ J_{\vec{k}\vec{k}'} &= -V_{\vec{k}} V_{\vec{k}'} \left(\frac{1}{\varepsilon_{\vec{k}} - (\varepsilon^d + U)} + \frac{1}{\varepsilon_{\vec{k}'} - (\varepsilon^d + U)} - \frac{1}{\varepsilon_{\vec{k}} - \varepsilon^d} - \frac{1}{\varepsilon_{\vec{k}'} - \varepsilon^d} \right) \end{aligned} \tag{21}$$

since the local low energy sector is only comprised of the two singly occupied spin states $|\sigma\rangle$ while $|0\rangle, |2\rangle \in P_H$.

For a constant hybridization $|V_{\vec{k}}|^2 = V^2$ and conduction band energies close to the Fermi energy, $\varepsilon_{\vec{k}}$ can be neglected, and $J_{\vec{k}\vec{k}'} \to J = -2V^2 U/[\varepsilon^d(\varepsilon^d + U)] > 0$ for the local moment regime where $\varepsilon^d < 0$ and $\varepsilon^d + U > 0$. At the particle-hole symmetric point $\varepsilon^d = -U/2$ the dimensionless Kondo coupling $\rho J = 8\Gamma_0/(\pi U)$ determines the charge fluctuation scale at, where $\Gamma_0 = \Gamma(0)$.

We have demonstrated that the Schrieffer-Wolff transformation generates an effective Kondo Hamiltonian for the low energy sector of the SIAM in second order in the hybridization. This clearly reveals the connection between the SIAM, which includes all orbital and spin degrees of freedom, and the Kondo model focusing solely on the local spin degrees of freedom. The numerical renormalization group approach [10, 11], discussed in the lecture of R. Bulla, is able to explicitly track the flow from a free-orbital fixed point for $\beta = 1/T \to 0$ to the Kondo model at intermediate temperatures $T/\Gamma_0 \approx 0.1$ and odd integer fillings of the orbital by iteratively eliminating the high energy degrees of freedom, which involve charge fluctuations.

More realistic descriptions of $3d$ and $4f$-shell dynamics requires more than one orbital. H_{imp} is easily generalized from a single to many orbitals:

$$H_{imp} = \sum_{i\sigma} \varepsilon^d_i n^d_{i\sigma} + \sum_{\substack{\sigma\sigma' \\ mnpq}} U_{mnpq} d^{\dagger}_{n\sigma} d^{\dagger}_{m\sigma'} d_{p\sigma'} d_{n\sigma} \,. \tag{22}$$

The direct and exchange Coulomb matrix elements U_{mnpq} will differ but are related by symmetry in the absence of relativistic effects, such as the spin-orbit interaction. This is discussed in more detail in the lecture of R. Eder. The Coulomb interaction in H_{imp} takes the rotational invariant form

$$
\begin{aligned}
H^U & = \frac{U}{2} \sum_{i\sigma} n_{i\sigma}^d n_{i-\sigma}^d + \frac{2U'-J}{4} \sum_{\substack{m \neq m' \\ \sigma\sigma'}} n_{m\sigma}^d n_{m'\sigma'}^d - J \sum_{m \neq m'} \vec{S}_m \vec{S}_{m'} \\
& \quad - \frac{J}{2} \sum_{\substack{m \neq m' \\ \sigma}} d_{m\sigma}^\dagger d_{m-\sigma}^\dagger d_{m'-\sigma} d_{m'\sigma}
\end{aligned}
\tag{23}
$$

in spin-space by identifying $U_{nnnn} = U$, $U_{nmmn} = U - 2J = U'$, $U_{nmnm} = J$, $U_{nnmm} = -J$. Clearly, neglecting the orbital pair-transfer term $d_{m\sigma}^\dagger d_{m-\sigma} d_{m'-\sigma} d_{m'\sigma}$ breaks this rotational invariance. Since $J > 0$, the $\vec{S}_m \vec{S}_{m'}$ term is responsible for the Hund's rules, which favor the maximizing of the local spin and of the angular momentum by a ferromagnetic alignment.

2 Renormalization group

We have learned several important points in the previous sections: (i) The low energy physics of the Kondo effect shows universality and is characterized by a single energy scale T_K. (ii) The universality suggests that the problem can be tackled by approaches which were developed in the context of phase transitions: the renormalization group approach. (iii) The perturbative analysis breaks down due to infrared divergencies.

These divergencies indicate that the ground state of the starting point, a free conduction band coupled to a single spin, is orthogonal to the ground state of the strong-coupling fixed-point which governs the low energy physics.

2.1 Anderson's poor man's scaling

This section covers the simplest perturbative renormalization group (RG) approach to the Kondo model developed by Anderson [12] 1970. Although it does not solve the problem, it sets the stage for the deeper understanding of the physics provided by Wilson's numerical renormalization group approach.

We begin with the definition of s-wave conduction band annihilation operators $c_{\varepsilon\sigma}$

$$
c_{\varepsilon\sigma} = \sqrt{\frac{1}{N\rho(\varepsilon)}} \sum_{\vec{k}} \delta(\varepsilon - \varepsilon_{\vec{k}}) c_{\vec{k}\sigma} \,,
\tag{24}
$$

which are obtained by angular integrating on a shell of constant energy ε. Starting from the anti-commutator $\left\{ c_{\vec{k}\sigma}, c_{\vec{k}'\sigma'}^\dagger \right\} = \delta_{\sigma\sigma'} \delta_{\vec{k},\vec{k}'}$ of a discretized system, the prefactor $[\sqrt{N\rho(\varepsilon)}]^{-1}$ ensures the proper normalization of

$$
\left\{ c_{\varepsilon\sigma}, c_{\varepsilon'\sigma'}^\dagger \right\} = \delta_{\sigma\sigma'} \delta(\varepsilon - \varepsilon')
\tag{25}
$$

in the continuum limit since the density of state $\rho(\varepsilon)$ is defined as

$$\rho(\varepsilon) \;=\; \frac{1}{N} \sum_{\vec{k}} \delta(\varepsilon - \varepsilon_{\vec{k}}) \,. \tag{26}$$

By supplementing the δ-function with some suitable symmetry adapted form factor $B(\vec{k})$, $\delta(\varepsilon - \varepsilon_{\vec{k}}) \to \delta(\varepsilon - \varepsilon_{\vec{k}})B(\vec{k})$, such as a spherical harmonics $Y_{lm}(\Omega)$ or a Fermi surface harmonics [13], we could generalize these operators to the appropriate symmetry beyond simple s-wave scattering considered here. With those operators, the Hamiltonian (1) takes on the continuous form

$$H = \sum_\sigma \int_{-\infty}^{\infty} d\varepsilon \; \varepsilon c_{\varepsilon\sigma}^\dagger c_{\varepsilon\sigma} + \int_{-\infty}^{\infty} d\varepsilon \int_{-\infty}^{\infty} d\varepsilon' J(\varepsilon,\varepsilon') \sum_{\alpha\beta} c_{\varepsilon\alpha}^\dagger \vec{\sigma} c_{\varepsilon'\beta} \vec{S}_{imp} \tag{27}$$

where we have defined $J(\varepsilon,\varepsilon') = \frac{1}{2}J\sqrt{\rho(\varepsilon)\rho(\varepsilon')}$.

This formulation is still very general. It turns out, however, that the occurrence of the infrared divergence is linked to finite density of states at the Fermi energy. For simplicity, we assume a constant density of states restricted to the interval $\varepsilon \in [-D, D]$. $\rho_0 = 1/(2D)$ on this energy interval, and the Fermionic operator c_ε has the dimension of $1/\sqrt{E}$. After introducing the dimensionless coupling constant $g = \rho_0 J/2$, the dimensionless energy $x = \varepsilon/D$ and the dimensionless operators $c_{x\sigma} = \sqrt{D}c_{\varepsilon\sigma}$, we obtain the dimensionless isotropic Kondo Hamiltonian

$$\tilde{H} = \frac{H}{D} = \sum_\sigma \int_{-1}^{1} dx \; x c_{x\sigma}^\dagger c_{x\sigma} + g \int_{-1}^{1} dx \int_{-1}^{1} dx' \sum_{\alpha\beta} c_{x\alpha}^\dagger \vec{\sigma} c_{x'\beta} \vec{S}_{imp} \tag{28}$$

which will be subject to a perturbative renormalization group treatment. Since $\delta(\varepsilon - \varepsilon') = \delta([x - x']D) = \delta(x - x')(1/D)$, the rescaled operators also obey a normalized anti-commutator relation

$$\{c_{x\sigma}, c_{x'\sigma'}^\dagger\} \;=\; (\sqrt{D})^2 \{c_{\varepsilon\sigma}, c_{\varepsilon'\sigma'}\} = D\delta_{\sigma\sigma'}\delta(\varepsilon - \varepsilon') = \delta_{\sigma\sigma'}\delta(x - x') \,. \tag{29}$$

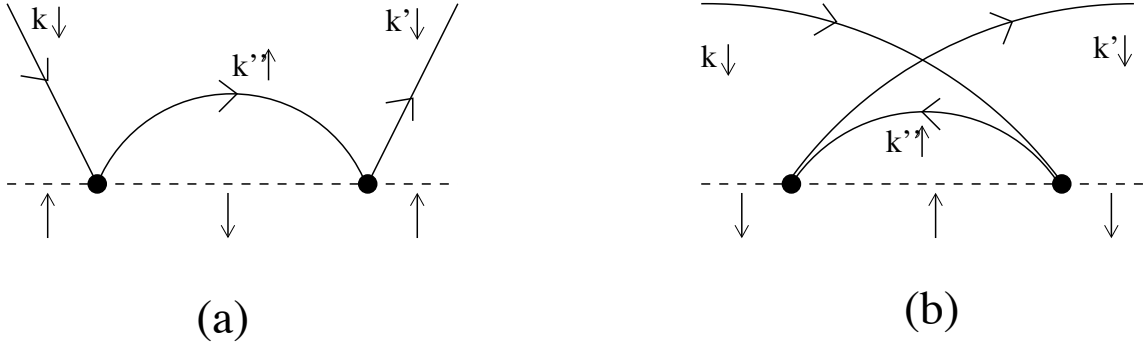The key ingredients to any renormalization group (RG) transformation are

1. separation of energy scale

2. eliminating high energy contributions by renormalizing low energy coupling constants

3. rescaling of all parameters and quantum fields

In the first step we define the appropriate low and high energy sector $\hat{P}_L$ and $\hat{P}_H = 1 - \hat{P}_L$ by partitioning the Fock-space appropriately. In the second step we perform the same transformations as outlined in Eq. (19). By eliminating the coupling between these sectors up to quadratic order, the effective Hamiltonian of the low energy subspace

$$H'_{LL} = \hat{P}_L H' \hat{P}_L = \hat{P}_L H \hat{P}_L + \hat{P}_L \frac{\lambda^2}{2}[S, \bar{V}]\hat{P}_L + O(\lambda^3) = H_{LL} + \Delta H_{LL}^{(2)} + O(\lambda^3) \tag{30}$$

acquires renormalized parameters via virtual transitions between the low and the high energy sectors mediated by V up to the second order in λ.

Fig. 1: *The particle (a) and the hole (b) spin-flip processes in second order in J contributing to the renormalization of J.*

Since the procedure is rather trivial for the free electron gas, we illustrate the steps on this part of the Hamiltonian. We introduce a dimensionless parameter $s > 1$ and split H_b into two contributions:

$$\frac{H_b}{D} = \sum_\sigma \int_{-1/s}^{1/s} dx \; x c_{x\sigma}^\dagger c_{x\sigma} + \sum_\sigma \left(\int_{-1}^{-1/s} dx + \int_{1/s}^1 dx \right) x \, c_{x\sigma}^\dagger c_{x\sigma} \,. \tag{31}$$

One contribution contains all low energy modes $|x| < 1/s$ and the other all high energy modes $1/s < |x| < 1$. Defining $\hat{P}_L$ as the operator which projects onto all modes $|x| < 1/s$, the Hamiltonian is written as $H_b = \hat{P}_L H_b \hat{P}_L + \hat{P}_H H_b \hat{P}_H$ and, therefore, $V = 0$. Focusing on the low energy part

$$H_b' = H_{LL} = \hat{P}_L H_b \hat{P}_L = \sum_\sigma \int_{-1/s}^{1/s} dx \; x \, c_{x\sigma}^\dagger c_{x\sigma} \tag{32}$$

we have to rescale the energy modes x to $x' = sx$ in order to restore the original mode distribution $|x'| < 1$ and obtain

$$H_b' = \sum_\sigma s^{-2} \int_{-1}^1 dx' \; x' c_{x(x')\sigma}^\dagger c_{x(x')\sigma} \,. \tag{33}$$

Since original Fermionic operators have the dimension $1/\sqrt{E}$, they must also be scaled as $c_{x'} = \sqrt{s} c_{x(x')\sigma}$ on expansion of the scale from $1/s \to 1$, which leads to

$$H_b' = \frac{1}{s} \sum_\sigma \int_{-1}^1 dx' \; x' c_{x'\sigma}^\dagger c_{x'\sigma} \,. \tag{34}$$

This completes the third and last step of the RG procedure.

The dimensionful Hamiltonian H_b remains invariant under the mode elimination procedure if $H_b/D = H_b'/D'$. Comparing the rescaling of the integrals and fields after the mode elimination, Eq. (34) yields the scaling equation of the band width: $D' = D/s$. Such an invariance is called a fixed point under the RG transformation, and the Hamiltonian of the free electron gas is obviously such a fixed point Hamiltonian.

Before we come back to the Kondo interaction, we briefly review the scaling of an additional local Coulomb interaction $H_U \propto c^\dagger_{x_1\sigma} c^\dagger_{x_2\sigma'} c_{x_3\sigma'} c_{x_4\sigma}$ under the RG transformation. Performing the same RG steps in linear order, we accumulate $[s^{1/2}]^4$ for the rescaling of the four fields and $[s^{-1}]^4$ for the four integral transformation, s^{-2} in total. The Coulomb interaction is irrelevant since it vanishes under the RG flow. As a consequence, we, therefore, expect a local Fermi-liquid with vanishing scattering cross sections $\propto \omega^2$ at $T \to 0$, described by the strong-coupling fixed-point. Since we have understood the transformation of the free electron gas, we can add the dimensionless Kondo interaction H_K

$$H_K = \frac{1}{2} \sum_{\alpha,\beta} \sum_{i=x,y,z} \int_{-1}^{1} dx_1 \int_{-1}^{1} dx_2 \, c^\dagger_{x_1\alpha} c_{x_2\beta} \, g^i \underline{\underline{\sigma}}^i_{\alpha\beta} \tau^i \,, \tag{35}$$

to the H_b and investigate $H = H_b + H_K$ under this RG transformation. In this expression, the local spin is represented by $\vec{S}_{loc} = \vec{\tau}/2$ and $g = \rho_0 J/2$ is generalized to three components g^i which include the anisotropic Kondo models.

Performing the unitary transformation (20), the low energy sector of H_K contributes to H in linear order via $\Delta H_d = \hat{P}_L H_{int} \hat{P}_L + \hat{P}_H H_{int} \hat{P}_H$. Additionally it generates the off-diagonal part $V = \hat{P}_L H_K \hat{P}_H + \hat{P}_H H_K \hat{P}_L$ for the Schrieffer-Wolff type transformation. Since the term linear in g, ΔH_d is invariant under the RG transformation, H_K is called a marginal operator in the vicinity of the local moment fixed point defined by $H_K = 0$.

In order to decide whether it is a relevant or irrelevant marginal operator, we have to go to second order in g. Using the eigenstates of H_d, $|p\rangle$ of the low-energy and $|q\rangle$ of the high-energy sector of the Fock space, we derive with the condition, $[S, H_d] = -V$
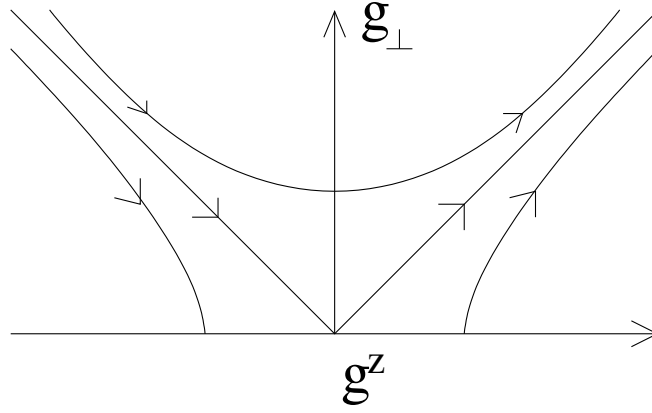
$$\Delta H^{(2)}_{LL} = \sum_{p,p'} |p\rangle\langle p'| \frac{1}{2} \sum_q V_{pq} V_{qp'} \left(\frac{1}{E_p - E_q} + \frac{1}{E_{p'} - E_q} \right) \,. \tag{36}$$

H_K contains a spin-spin interaction bilinear in the conduction electron operators. Therefore, one of the operators in $c^\dagger_{x_1\alpha} c_{x_2\beta}$ must contain a high-energy particle or hole excitation in V which is connected with the same conduction electron mode to one conduction electron line integrated out by mode elimination. Those matrix elements of $\Delta H^{(2)}_{LL}$ can be calculated diagrammatically using the two diagrams depicted in Fig. 1(a) and (b). Again, we eliminate a very thin shell of high energy excitations of width $\Delta l = 1 - 1/s = -\Delta D/D$, and the two diagrammatic contributions yield the quadratic corrections to g^i

$$\Delta H^{(2)}_{LL} = \Delta l \sum_{\alpha\beta} \int_{-1/s}^{1/s} \int_{-1/s}^{1/s} dx_1 dx_2 \, c^\dagger_{x_1\alpha} c_{x_2\beta} \, (g^x g^y \tau^z \sigma^z + g^y g^z \tau^x \sigma^x + g^x g^z \tau^y \sigma^y) \,. \tag{37}$$

In the derivation of these equations, we have used the eigenstates of H_b and neglected the correction generated by H_K. This is a further approximation since the construction of S requires eigenstates of H_d and not only of H_b. This clearly restricts the validity of the flow equations derived below to small values of g^i.

The flow of the effective band width $dD/D = -dl$ is used to eliminate Δl. The combination of the infinitesimal change $\Delta H^{(2)}_{LL}$ in the limit $\Delta l \to dl$ with the linear contribution of H_K to the

Fig. 2: *Flow of the coupling constants g^z and $g_\perp$, which is given by a set of hyperbolic curve as show in Eq. (39). For transverse coupling $|g_\perp| > g_z$, the Kondo coupling always flows to the strong-coupling fixed-point $g^z, g_\perp \to \infty$. For a ferromagnetic $g^z < 0$, $g_\perp$ renormalized to $g_\perp = 0$ where the RG-flow stops.*

low-energy sector, $P_L H_K P_L$, yields the three perturbative RG equations

$$\frac{dg^x}{d\ln\mathcal{D}} = -2g^y g^z \tag{38a}$$

$$\frac{dg^y}{d\ln\mathcal{D}} = -2g^x g^z \tag{38b}$$

$$\frac{dg^z}{d\ln\mathcal{D}} = -2g^x g^y \tag{38c}$$

for the parameter flow of the coupling constants. Fixed points of those flow equations are defined by $dg^i/d\ln\mathcal{D} = 0$ for all $i = x, y, z$. These equations are called poor man's scaling in the literature.

In the transversal Kondo model defined by two independent parameters g^z and $g_\perp = g^x = g^y$ these equations reduce to

$$\frac{dg_\perp}{d\ln\mathcal{D}} = -2g_\perp g^z \quad ; \quad \frac{dg^z}{d\ln\mathcal{D}} = -2g_\perp^2 \,, \tag{39}$$

from which we obtain by integration $[g^z]^2 - g_\perp^2 = \text{const}$. Therefore, the flow of the parameters g^z and $g_\perp$ are located on a hyperbolic curve in the parameter space $(g^z, g_\perp)$ which is depicted in figure 2. Since the RG-flow in Eq. (39) alway stops when $g_\perp$ vanishes, $(g^z, 0)$ defines a line of fixed points for $[g^z]^2 - g_\perp^2 > 0$ and $g^z < 0$. If the transverse coupling is larger than the ferromagnetic coupling g^z, $g^z < 0$, the transversal coupling $g_\perp$ remains finite for $g^z = 0$ and induces a sign change of g^z. The couplings flow to the strong-coupling fixed-point $(g_\perp, g^z) \to (\infty, \infty)$. These flow equations have one stable fixed point $(g^z, g_\perp) = (\infty, \infty)$ and one line of fixed points $(g^z, 0)$. The latter are stable for a ferromagnetic $g_z < 0$ and unstable for $g_z > 0$. For a fully isotropic Kondo coupling, $g = g^z = g_\perp$, we only need to integrate the single differential equation

$$\frac{dg}{d\ln\mathcal{D}} = \beta(g) = -2g^2 \,. \tag{40}$$

The function $\beta(g)$ is called the β-function in the literature and determines how the coupling constants flow while reducing the band width: a negative β-function is a signature of weak interactions at high-energies and a growing interaction strength while reducing the band width. With the initial values of the model D_0, g_0, we integrate this differential equation to

$$g(D') = \frac{g_0}{1 + 2g_0 \ln(D_0/D')} \, . \tag{41}$$

This solution obviously breaks down at a low energy scale $T_K = D$ at which the denominator diverges:

$$T_K = D_0 e^{-1/2g_0} = D_0 e^{-1/\rho_0 J} \, . \tag{42}$$

However, the poor-man scaling approach is only valid for small coupling constants g, since higher order processes will modify the β-function. Nevertheless, we can use the new energy scale to express the running coupling constant $g(\mathcal{D}')$ as function of T_K

$$g(D') = \frac{1}{\ln(D'/T_K)} \tag{43}$$

which removes all reference to the original parameters. The coupling constant became an universal function of the ratio between cutoff and the new characteristic low energy scale T_K.

How can we understand the divergence of the effective coupling constant? If we let $g \to \infty$, we can ignore the kinetic energy of the conduction electrons for a moment and focus on the local Kondo interaction (35):

$$H_K = \frac{1}{2} \sum_{\alpha,\beta}^{\mu=x,y,z} c_{0\alpha}^\dagger c_{0\beta} g^\mu \underline{\underline{\sigma}}_{\alpha\beta}^\mu \tau^\mu \, , \tag{44}$$

where $c_{0\sigma} = \int_{-1}^{1} dx c_{x\sigma}$. Since H_K conserves spin and charge, a singlet and a triplet state is formed for $n_c = 1$, while the empty and doubly occupied conduction electron state does not couple to the local spin. The singlet has the energy of $-3/2g$, the three triplet states lie at the energy $g/2$ and the other two at $E = 0$. In the anti-ferromagnetic case $g > 0$, the ground state is a singlet, which is energetically decoupled from the rest of the conduction electrons for $g \to \infty$. The ground state in this strong-coupling limit will be a free electron gas with one electron removed and absorbed into this bound state. Hence, the ground state is orthogonal to the ground state of the local moment fixed point we started with. That is the reason why these ground states cannot be connected via perturbation theory. Since the scattering turns out to be irrelevant in the vicinity of this so-called strong-coupling fixed-point, it is a stable fixed point under the RG transformation.

Although the presented perturbative RG fails to solve the Kondo problem, it already proves that the original Kondo Hamiltonian is unstable in second order of g and predicts the correct crossover scale T_K. However, the divergence of the coupling constant happens already at a finite cutoff $D = T_K$ which must be an artifact of the approximation used since the model cannot have any phase transition at finite temperature. The correct solution can only be obtained by the numerical renormalization group [14, 15] or the Bethe ansatz [16].

2.2 Wilson's numerical renormalization group approach

Although Anderson's perturbative RG has already provided some deeper physical insight, its perturbative nature restricts its validity to a close range around its starting point: it cannot access the crossover regime from high to low temperature.

The Hamiltonian of a quantum impurity system is generally given by

$$H = H_{\text{bath}} + H_{\text{imp}} + H_{\text{mix}} , \qquad (45)$$

where H_{bath} models the continuous bath, H_{imp} represents the decoupled impurity, and H_{mix} accounts for the coupling between the two subsystems.

Such a system can be accurately solved using Wilson's numerical renormalization group (NRG) [14, 15]. At the heart of this approach is a logarithmic discretization of the continuous bath, controlled by the discretization parameter $\Lambda > 1$. The continuum limit is recovered for $\Lambda \to 1$. Using an appropriate unitary transformation, the Hamiltonian is then mapped onto a semi-infinite chain, with the impurity coupled to the open end. The nth link along the chain represents an exponentially decreasing energy scale: $D_n \sim \Lambda^{-n/2}$ for a fermionic bath [14] and $D_n \sim \Lambda^{-n}$ for a bosonic bath [17]. Using this hierarchy of scales, the sequence of dimensionless finite-size Hamiltonians

$$
\begin{aligned}
\Lambda^{-(N-1)/2} H_N \;=\; & \frac{2}{D\,(1+\Lambda^{-1})}(H_{\text{imp}} + H_{\text{mix}}) \\
& + \sum_{\alpha}\sum_{n=0}^{N} \Lambda^{-(n-1)/2}\, \bar{\varepsilon}_{n\alpha} f_{n\alpha}^{\dagger} f_{n\alpha} \\
& + \sum_{\alpha}\sum_{n=0}^{N-1} \Lambda^{-n/2}\, \bar{t}_{n\alpha}(f_{n\alpha}^{\dagger} f_{n+1\alpha} + f_{n+1\alpha}^{\dagger} f_{n\alpha})
\end{aligned}
\qquad (46)
$$

for the N-site chain is solved iteratively, discarding the high-energy states at the conclusion of each step to maintain a manageable number of states. This reduced basis set of H_N is expected to faithfully describe the spectrum of the full Hamiltonian on a scale of D_N, corresponding to a temperature $T_N \sim D_N$.

Note that the dimensionless energies $\bar{\varepsilon}_{n\alpha}$ and tight-binding parameters $\bar{t}_{n\alpha}$ are of the order $O(1)$. In general, α labels all independent flavor and spin degrees of freedoms of the bath Hamiltonian. In the case of the single-band Kondo model, α denotes only the two spin states of the conduction electron band. The parameters $\bar{\varepsilon}_{n\alpha}$ and $\bar{t}_{n\alpha}$ encode all relevant details of a non-constant density of states.

Therefore, the NRG can be applied to pseudo-gap systems and used as an impurity solver for the dynamical mean field theory where in the self-consistently obtained coupling function $\Gamma(\omega)$ the lattice information and the formation of a Mott-Hubbard insulator is encoded [15]. The details on the connection between the coupling function $\Gamma(\omega)$ and the NRG parameters $\bar{\varepsilon}_{n\alpha}$ and $\bar{t}_{n\alpha}$ will be connected in R. Bulla's subsequence lecture.

We have followed the notation of Ref. [10, 11] where a mapped bath electron of flavor α is created (annihilated) by $f_{n\alpha}^{\dagger}(f_{n\alpha})$ at chain link n while in Bulla's lecture $c_{n\sigma}^{\dagger}(c_{n\sigma})$ is used for the

same operators. We also defined the Hamiltonian H_N in accordance with the original literature, while Bulla kept the factor $D/[2(1 + \Lambda^{-1})]$ in his definition of H_N. We also emphasize the energy hierarchy by making the exponential decay of the tight binding parameters explicitly. The dimensionless parameters $\bar{\varepsilon}_{n\alpha}$ and $\bar{t}_{n\alpha}$ and those used in Bulla's lecture are connected by

$$\varepsilon_n = \frac{D\,(1 + \Lambda^{-1})}{2}\Lambda^{-(n-1)/2}\,\bar{t}_{n\alpha} \tag{47a}$$

$$t_n = \frac{D\,(1 + \Lambda^{-1})}{2}\Lambda^{-n/2}\,\bar{t}_{n\alpha} \tag{47b}$$

Due to the exponential form of the Boltzmann factors in the density operator, $\hat{\rho} = \exp(-\beta H)/Z$, the reduced NRG basis set of $\mathcal{H}_N$ is sufficient for an accurate calculation of thermodynamic quantities at temperature T_N. The fixed points under the RG transformation

$$H_{N+1} = \sqrt{\Lambda}H_N + \sum_\alpha \left(\bar{\varepsilon}_{N+1\alpha}f^\dagger_{N+1\alpha}f_{N+1\alpha} + \bar{t}_{N\alpha}(f^\dagger_{N\alpha}f_{N+1\alpha} + f^\dagger_{N+1\alpha}f_{N\alpha}) \right) \tag{48}$$

determines the thermodynamics properties and allows deep insight into the physics of the system. In SIAM, they have been explicitly stated in Refs. [10, 11]. It has been shown [14] that the Kondo temperature indeed determines the crossover scale from the local moment fixed point to the strong-coupling fixed-point. T_K is the only relevant energy scale at low temperatures so that all physical properties can be obtained from universal scaling functions for T/T_K and $\omega/T_K < 1$.

More details on the NRG and its power can be found in the lecture by R. Bulla or the NRG review [15] he co-authored.

2.3   Exotic Kondo effects in metals

In the previous section we have focused on the simplest case of a single spin-degenerate band coupled anti-ferromagnetically to a single local spin $S = 1/2$. The Kondo temperature T_K defines the crossover scale below which a singlet ground state emerges and the local spin is asymptotically screened.

How does the physics change if we couple a local spin with $S > 1/2$ to a single conduction band, or a spin $S = 1/2$ to more than one spin-degenerate conduction electron band?

We have discussed above that a Kondo Hamiltonian can be derived as an effective low energy Hamiltonian by applying a Schrieffer-Wolff (SW) transformation to the SIAM. If we consider its multi-orbital extension, Eq. (22), a much richer variety of impurity ground states emerge after freezing out the charge fluctuations. In Mn, Co, or other transition metal ions, Hund's rules generate a ground state spin $S > 1/2$, while point group symmetries in lattices or ligand symmetries in molecules [18] can suppress the hybridization to more than one conduction band. After a SW-transformation we could end up with an under-compensated Kondo model, schematically depicted in Fig. 3(c). The single conduction electron band will partially screen the local spin S to an effective spin $S' = S - 1/2$ which asymptotically decouples from the conduction band. It turns out that the RG fixed point is similar to the strong-coupling fixed-point,

but with a degeneracy of $2S$ remaining. The remaining very weakly coupled magnetic scatterer significantly modifies the universal functions describing the physical properties at temperatures $T < T_K$, and corrections to the T^2 behavior of a Fermi liquid are found. Hence, it is also called a singular Fermi-liquid which is characterized by a residual impurity entropy $S_{\mathrm{loc}} = \log(2S)$. The impurity entropy S_{loc} is defined as the difference of the total entropy and the entropy of the conduction band without impurity.
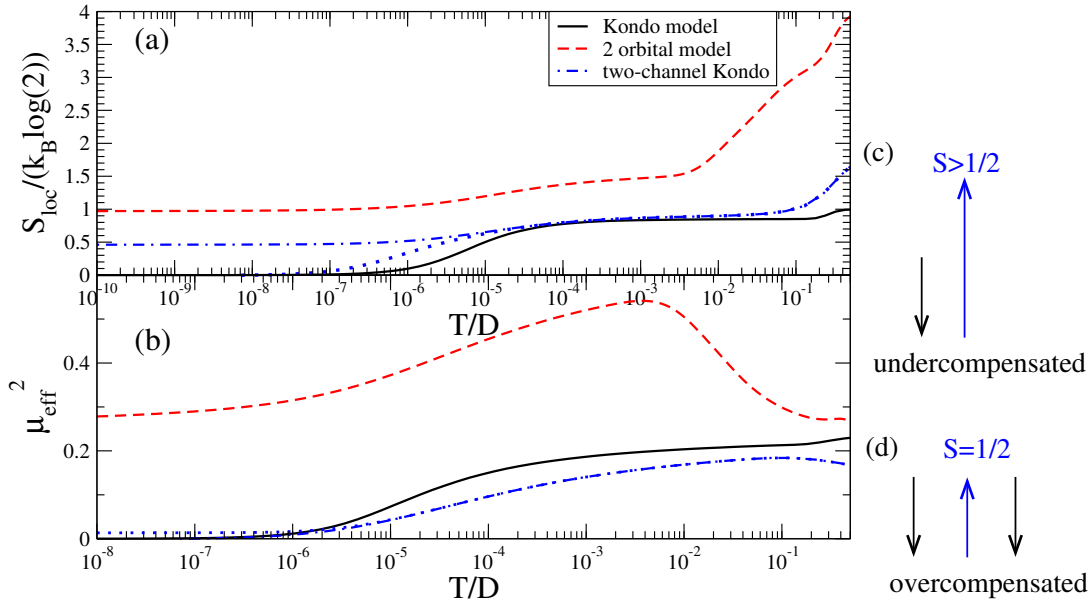
In the overcompensated Kondo model ($M > 1$)

$$H_K = \sum_{\alpha=1}^{M} J_\alpha \vec{S}\vec{s}_{b,\alpha} \, , \tag{49}$$

no Kondo singlet ground state can be formed by the local $S = 1/2$ impurity spin and the local conduction electron spins $\vec{s}_{b,\alpha}$, a consequence of the flavor conservation in such models. However, such flavor conservation is very hard to obtain from the SW transformation and might only occur in very exotic systems due to symmetry restrictions. Such models are characterized by an additional unstable intermediate-coupling fixed-point which can be understood by a simple argument: In very weak coupling $g_\alpha = \rho_0 J_\alpha/2 \to 0$, the poor man's scaling is applicable and g_α increases as we have discussed in the previous section. However, in the opposite limit, $1/g_\alpha \to 0$, we only need to consider one localized conduction electron in each channel α coupled to the local spin and treat the kinetic energy as perturbation. The ground state for anti-ferromagnetic g is formed by a composite $S' = M - S$ spin, which remains coupled to the rest of the conduction electrons by an effective matrix element of the order of the band width. Hence, an effective Kondo model is generated in which the coupling has been reduced from $g_\alpha \gg 1$ to $g_{\mathrm{eff}} \approx 1$. A detailed analysis proves [19] that the large coupling flows to smaller couplings, and the small couplings increase. Hence, both must flow to a fixed point of intermediate coupling strength. This requires the inclusion of the third order contributions to the β-function in Eq. (40). In the case of the isotropic two-channel Kondo model, $S = 1/2$ and $M = 2$, it takes the simple form $\beta(g) = -g^2 + g^3$ for a uniform Kondo coupling. In addition to the trivial fixed-point, $g = 0$, it has an intermediate fixed-point $\beta(g_c = 1) = 0$ [19]. It is interesting to note that the intermediate-coupling fixed-point impurity entropy reaches $(k_B/2)\log(2)$, indicating that a Majorana fermion decouples [20] from the system in the low energy limit. However, this fixed point is unstable against breaking of channel and spin symmetry. Under channel symmetry breaking, i.e. $J_1 \neq J_2$, the RG flow renormalizes $J_{\mathrm{max}} = \max(J_1, J_2) \to \infty$ and $J_{\mathrm{min}} = \min(J_1, J_2) \to 0$: the channel with the larger coupling forms a normal Kondo singlet while the other channel decouples.

In Fig. 3(a), the temperature dependent local entropy S_{loc} for the three cases, the compensated (black), the under-compensated (red) and the overcompensated (blue) model is depicted. For the compensated Kondo model, $S_{\mathrm{loc}} \approx k_B \log(2)$ at high temperature, which is reduced to $S_{\mathrm{loc}} \to 0$ for $T \to 0$ indicating the Kondo singlet formation. This corresponds to a vanishing effective local moment on the temperature scale $T_K \approx 10^{-5}D$.

The under-compensated model presented here comprises of a two-orbital Anderson model with a ferromagnetic Hund's rule coupling in Eq. (22), coupled to single conduction electron band.

Fig. 3: *(a) Impurity entropy of the $S = 1/2$ Kondo model (black line), the under-compensated $S = 1$ model (red line) and the two-channel Kondo model (blue) line. (b) The local effective moment μ_{eff}^2 defined as $\mu_{\text{eff}}^2 = \langle S_z^2 \rangle_H - \langle S_z^2 \rangle_{H_b}$ for the same three models as in (a). (c) the local $S > 1/2$ coupled to one conduction spin is under-compensated, (d) a spin $S = 1/2$ is coupled to two conduction bands which is described by the two-channel Kondo model.*

For $T \to \infty$, the free orbital fixed point is 2^4-fold degenerate resulting in $S_{\text{loc}}(\beta = 0) = 4k_B \log(2)$. As depicted in Fig. 3(a), it approaches $k_B \log(2)$ for $T \to 0$, indicating an un-screened decoupled $S = 1/2$ degree of freedom.

$S_{\text{loc}}(T)$ for the overcompensated two-channel Anderson model [21–23] is shown as a blue curve. Starting from 4-fold degenerate local orbital fixed point, an effective two-channel Kondo model is found in the interval $10^{-3} < T/D < 10^{-1}$, and approaches the intermediate-coupling two-channel Kondo fixed point value of $S_{\text{loc}} \approx k_B \log(2)/2$. By applying a weak external magnetic field of $H = 10^{-4} \Gamma_0$, the two-channel symmetry is broken and a crossover to the strong-couping fixed point is observed – blue dotted line in Fig. 3(a). The crossover is governed by the scale $T^* \propto H^2/T_K$. The effective magnetic moment μ_{eff}^2 tracks the $H = 0$ curve up T^* and approaches a finite value induced by the finite magnetic field.

This model has originally been proposed by Cox [21] for uranium-based Heavy Fermions in which the U $5f$-shell is doubly occupied. It predicts an orbital Kondo effect where the non-magnetic Γ_3 doublet is screened by a four-fold degenerate Γ_8 conduction band. Experimentally, however, there is still no evidence for the realization of such a two-channel Kondo fixed point.

3 Kondo effect in lattice systems

3.1 Heavy Fermion materials

Heavy Fermions [24] are Ce and U based metallic compounds which show a strongly enhanced γ-coefficient of the specific heat. Typically an enhancement over simple Cu of a factor of $300 - 6000$ is found. Since $\gamma \propto m^*$ in a simple effective Fermi-liquid theory, the name Heavy Fermions was coined for this material class. It has been noted that the additional magnetic contribution to the specific heat scales with the number of magnetic ions upon substitution with non-magnetic elements such as La [24]. Apparently the major contribution in such strongly correlated materials stems from the electrons in the localized $4f$ or $5f$-shells. Early on, local approximations were proposed [25, 26] in which each Ce or U site is treated as an independent Kondo scatterer interacting with an averaged conduction band. Coherence is recovered by summing up all single particle scattering events on a periodic lattice [24].

The most simplified description starts from a singly occupied $4f$-shell of Ce. Employing Hund's rules, spin-orbit coupling yields a $J = 5/2$ ground state multiplet which is quenched by the lattice point group symmetry either to a quartet and doublet in cubic crystal, or three Kramers doublets in a tetragonal environment. Taking into account only a single Kramers doublet on each $4f$-shell and hybridizing the orbital with one effective conduction band defines the periodic extension of the Anderson model (PAM)

$$H = \sum_{i\sigma} \varepsilon_i^f f_{i\sigma}^\dagger f_{i\sigma} + U n_{i\uparrow} n_{i\downarrow} + \sum_{\vec{k}\sigma} \varepsilon_{\vec{k}\sigma} c_{\vec{k}\sigma}^\dagger c_{\vec{k}\sigma} + \sum_{i,\vec{k},\sigma} V_k \left(e^{i\vec{k}\vec{R}_i} f_{i\sigma}^\dagger c_{\vec{k}\sigma} + e^{-i\vec{k}\vec{R}_i} c_{\vec{k}\sigma}^\dagger f_{i\sigma} \right) , \quad (50)$$

where $f_{i\sigma}$ annihilates an f-electron at lattice site i with spin σ. Although this model can already explain some basic properties of HF materials [24], a more realistic description requires the full $J = 5/2$ ground state multiplet structure, since experimentally the influence of crystal-field effects are clearly seen in the specific heat or transport measurements [24].

As mentioned above, experimental evidence has indicated that the magnetic contribution to the specific heat scales with number of magnetic Lanthanide ions, hinting towards locally generated strong correlations. It was proposed that the single-particle dispersion can be calculated using a local t-matrix which accounts for all local correlations, while different lattice [25] sites are linked only by a free propagation of electrons. A physically intuitive picture emerges: at the chemical potential, the electrons are mainly trapped in local Kondo-resonances and propagate only rather rarely from site to site. On a larger length scale, a very slow coherent motion is generated which is equivalent to a quasi-particle with a large effective mass.

3.2 Dynamical mean field theory (DMFT)

The combination of local-density approximation (LDA) and DMFT for realistic description of material properties of a large variety of strongly correlated electron systems has been the topic of the last year's school [27] entitled *The LDA+DMFT approach to strongly correlated materials.*

In DMFT, the k-dependence of the lattice self-energy is neglected. The original idea for such a local approximation dates back to the mid 1980s [25, 26, 28] and has been applied to Heavy Fermion systems. In 1989, it was proven that such an approximation has an exact limit in infinite spatial dimensions [29–31] which broaden the applicability of this approximation to a much larger range of problems.

The basic idea of the DMFT [32, 33] can be summarized as follows: One picks out a single lattice site or a unit-cell. Instead of solving the local dynamics embedded in the full lattice exactly, which is usually not possible, the rest of the interacting lattice is replaced by a fictitious tight-binding model. This implies that two-particle and higher order correlation functions are treated as factorized, which imposes restrictions on the applicability of the theory to phase-transitions. This is augmented by a self-consistency condition (SCC) which equates the local lattice Green function $G_{\mathrm{lat}}(z)$

$$G_{\mathrm{lat}}(z) = \frac{1}{N}\sum_{\vec{k}} G_{\vec{k}}(z) = \frac{1}{N}\sum_{\vec{k}} \frac{1}{z - \varepsilon_{\vec{k}} - \Sigma(z)} = G_{\mathrm{loc}}(z) \tag{51}$$

with the local Green function $G_{\mathrm{loc}}(z)$ of such an effective site. This effective site of the DMFT is equivalent to an Anderson impurity model as defined in Sec. (1.2), and its local dynamics is determined by $G_{\mathrm{loc}}(z) = [z - \varepsilon^d - \Sigma(z) - \tilde{\Delta}(z)]^{-1}$. It requires the knowledge of the local orbital energy ε^d, the local Coulomb repulsion U and the hybridization function $\tilde{\Gamma}(\omega) = \Im m \tilde{\Delta}(\omega - i\delta)$. In the subsequent lecture by Bulla, the notation $\bar{\Delta}(z)$ will be used instead of $\Delta(z)$ $(\tilde{\Delta}(z))$ for a single impurity problem (effective DMFT site). Since $\Gamma(\omega)$ can be interpreted as energy dependent single orbital decay rate in the absence of any Coulomb interaction, we used the letter Γ in this lecture while Bulla denotes the same quantity as $\Delta(\omega)$. In the literature, both notations are found for the same quantity.

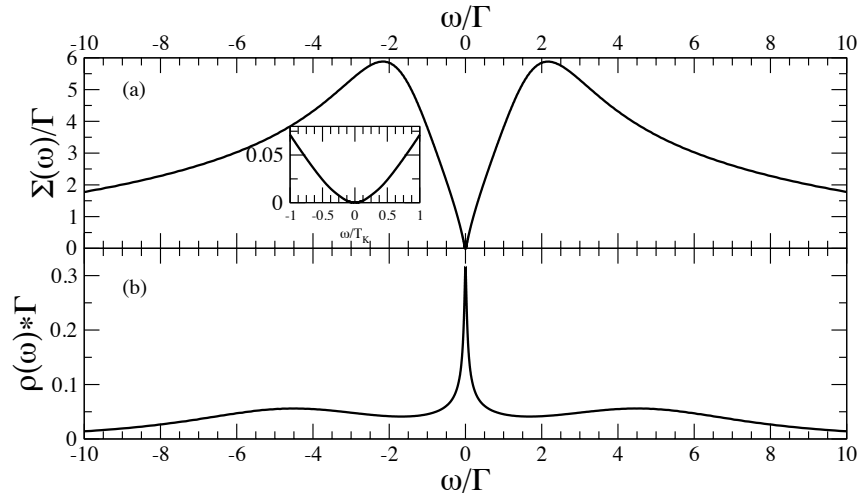For single band lattice models such as the PAM, Eq. (50), or the Hubbard model

$$H = \sum_{i\sigma} \varepsilon_i^d c_{i\sigma}^\dagger c_{i\sigma} - \sum_{ij} t_{ij}(c_{i\sigma}^\dagger c_{j\sigma} + c_{j\sigma}^\dagger c_{i\sigma}) + U n_{i\uparrow} n_{i\downarrow} \tag{52}$$

the effective site is given by Eq. (17) and can be easily extended to multi-orbital models [27] required for realistic transition metal compounds with partially filled $3d$-shells. In the latter case, Eq. (51) acquires a matrix form and the multi-orbital SIAM introduced in Sec. (1.2) is used to describe the effective site.

The self-consistent solution is obtained iteratively: after an initial guess of $\Delta(z)$, the dynamics of effective SIAM is calculated. Then its local self-energy $\Sigma(z)$ is used to obtain $G_{\mathrm{lat}}(z)$ via Eq. (51). Equating it with $G_{\mathrm{loc}}(z)$ yields a new $\tilde{\Delta}'(z)$ for the next step of the iteration. Usually convergence can be achieved in 10-20 iterations.

3.3 Impurity solver

It turns out that the k-summation in Eq. (51) is the computationally least expensive part of the DMFT iteration, even for multi-orbital problems. The calculation of local self-energy of a

Fig. 4: *(a) Impurity self-energy $\Sigma(\omega)$ and (b) spectral function for a symmetric single orbital Anderson impurity model with $\varepsilon^d = -5\Gamma, U = 10\Gamma$ and a symmetric featureless band of width $D = 30\Gamma$ calculated using the NRG [40] for $T = 0$. $T_K = 0.021\Gamma$. The inset in (a) shows the behavior of $\Sigma(\omega)$ for $|\omega/T_K| < 1$.*

single or multi-orbital SIAM remains the major challenge since the Kondo problem lies at the heart of these quantum impurity problems.

In the 1970s, it was shown that equation-of-motion techniques fail to describe the Kondo physics of the Anderson model. The perturbation expansion in U [34] was successful in accounting for the local Fermi liquid properties which develop adiabatically from the solution of the resonant level model. However, such conserving approximations [35,36] are not able to generate the correct energy scale T_K which is exponentially dependent on U; they remain restricted to the weakly correlated regime $U/(\pi\Gamma) \leq 1$. In the early 1980s, the non-crossing approximation [37–39] was developed. It starts out from the atomic limit and includes the local Coulomb interaction exactly. The hybridization is then considered as small compared to other energy scales, so it only included in the leading-order diagrams. Although this approach contains the correct energy scale up to some small correction, it remains essentially a high-temperature expansion, since the local Fermi-liquid is not described correctly. Friedel's sum rule is violated and the extracted $\Im m\Sigma(\omega - i\delta)$ becomes negative at low temperatures $T \ll T_K$. Only for the two-channel Anderson model, this approach yields remarkably good results [21,19] such as the correct power law of the self-energy.

Huge progress was made with the advent of quantum Monte Carlo algorithms [41] which yield, at least in principle, the correct dynamics. In practice, such approaches have two drawbacks: (i) they rely on a Trotter decomposition which limits the lowest accessible temperature. For typical parameters in high-temperature superconductors, this would often correspond to 500-1000K. (ii) The results are obtained on the imaginary time axis leaving an ill-defined problem of reconstructing the spectral function [42].

Nevertheless, new QMC approaches, based the expansion of the partition function Z rather
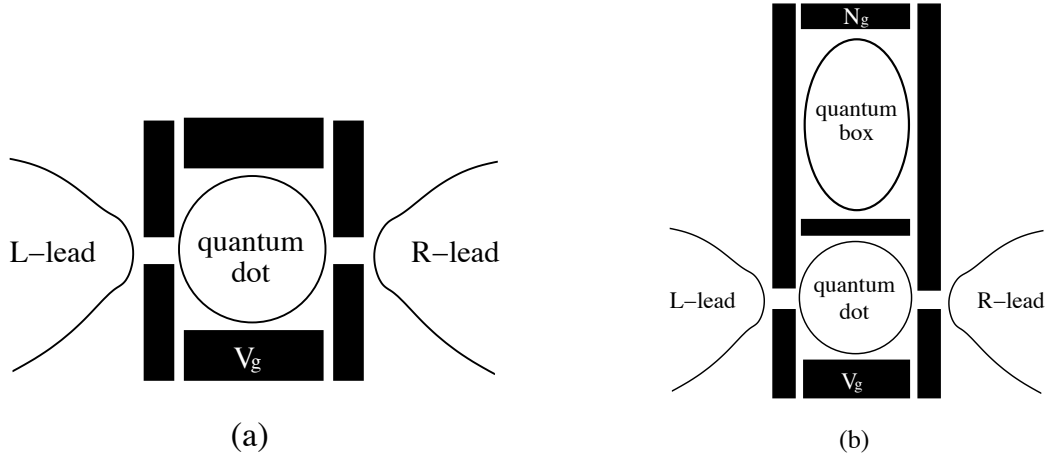
than on a Trotter decomposition, the so-called continuous-time QMC algorithms (CT-QMC) boosted the applicability range considerably and became standard within a few years (for a detailed comprehensive review see [43] and P. Werner's lecture in Ref. [27]). In the CT-QMC, the partition function Z is either expanded in the Coulomb-interaction, called the weak-coupling CT-QMC, or, similarly to the NCA, in the hybridization, called the strong-coupling CT-QMC. One of the big advantages of those solvers are that they scale very well with the number of the local orbitals. However, the sign problem of the fermionic determinants often restricts the applicability of QMC solvers to density-density type inter-orbital interactions, which breaks rotational invariance in spin-space.

Wilson's NRG has also been successfully employed as an impurity solver. While this approach includes the correct solution of any Kondo problem, the numerical effort scales exponentially with the number of conduction bands, which essentially limits the approach to two-band models, far from the five-band multi-orbitial models required, e.g., for FeAs based superconductors. A typical result for the dynamical properties of the single-orbital symmetric SIAM obtained using the NRG is shown in Fig. 4. The spectral function exhibits reminiscences of the two charge excitation peaks at $\omega \approx \varepsilon^d$ and $\varepsilon^d + U$ each carrying half of the spectral weight and are broadened by $2\Gamma(0)$. Clearly visible is a narrow peak called Kondo or Abrikosov-Suhl resonance.

The peak height is pinned to approximately $1/(\pi\Gamma(0))$ due to the Friedel sum rule [44]. We have discussed already that the strong-coupling fixed-point is a Fermi-liquid, since asymptotically the electron-electron scattering is freezing out for $|\omega| \to 0$. As a consequence, the imaginary self-energy shows a quadratic behavior $\Im m\Sigma(\omega - i\delta) \propto (\omega/T_K)^2$ for frequencies $(\omega/T_K)^2 \ll 1$ which is depicted in the inset of Fig. 4(a). Recovering a local Fermi-liquid on exponentially small energy scales $T_K \propto \exp(-1/\rho J_{\text{eff}})$ with a pinned resonance close to $\omega = 0$ in accordance with the Friedel sum rule remains the biggest challenge for any impurity solver. This low energy spectral behavior converts immediately into the quasi-particle band formation in the DMFT as can be seen from the analytic form of the lattice Green function $G_{\vec{k}}(z) = [z - \varepsilon_{\vec{k}} - \Sigma(z)]^{-1}$. For a true lattice solution, the full energy dependence of the self-consistently obtained hybridization function $\Gamma(\omega)$ plays a crucial role. This is neglected in Fig. 4 as it is beyond the scope of this lecture.

4   Kondo effect in nano-devices

In this section, a brief introduction to the Kondo-effect in nano-devices such as single-electron transistors (SET) is given. In the 1980s huge progress has been made in structuring semiconductors which opened new possibilities for designing nano-devices using semiconductor hetero-junctions. In 1998, David Goldhaber-Gordon demonstrate in a seminal paper [45] that the Kondo effect can also be observed in single-electron transistors [46]. We illustrate the connection to the Anderson model and also discuss how in larger quantum boxes a two-channel charge Kondo effect has been predicted by Matveev [47]. Combining a single-electron transistor with a quantum box might yield the first physical realization of a two-channel Kondo model [48].

Fig. 5: *(a) Schematic picture of a quantum dot which is weakly coupled to two leads. The filling of the confined region can be controlled by the gate voltage V_g. (b) Schematic picture of a quantum dot coupled to a larger quantum box and to two leads. The filling in the quantum box is controlled by N_g, the filling in the quantum dot is controlled by the gate voltage V_g.*

4.1   Kondo effect in single-electron transistors

A typical realization of a single-electron transistor is schematically depicted in Fig. 5(a). It consists of negatively charged gates which are added on top of an insulating layer covering a GaAs hetero-junction. Those gates partition the underlying 2D electron gas and confine some of the electron gas in smaller areas, forming the quantum dot. These confinement regions have a diameter of $d = 10 - 100$ nm, and their filling is controlled by a gate voltage. The tunneling matrix elements between the leads can be individually tuned by a set of gates. Nowadays, molecules and carbon nano-tubes are also used to form SETs, giving additional complexity due to their internal degrees of freedom. The single-particle levels in the confined area are discrete and randomly distributed. They can be characterized by a finite average level-spacing $\Delta\varepsilon$. The leading contribution from the Coulomb interaction is given by the classical charging energy of a capacitor $E_{\text{charge}} = (\hat{Q} - eN_g)^2/(2C) = (e^2/2C)(\hat{N} - N_g)^2$, where $\hat{Q} = e\hat{N}$ is the charge operator of the quantum dot, C its classical capacitance, and $N_g \propto V_g$ controls the filling. Then, the so-called constant interaction model for a quantum dot reads

$$H_{\text{dot}} = \sum_i \varepsilon_i \hat{n}_i + \frac{1}{2} E_c (\hat{N} - N_g)^2 \,, \tag{53}$$

where n_i is the number operator of the ith level with energy ε_i and the Coulomb interaction enters only via the charging energy $E_c = e^2/C$, ignoring the details of the individual single-electron wave functions.

At high temperatures $\langle \hat{Q} \rangle \propto V_g$, and we recover the classical limit. At low temperatures, $\beta E_c \gg 1$, the quantization of the charge becomes relevant. The transport through the quantum dot can only occur by single-electron hopping processes, from which the name single-electron transistor [46] was coined. At low temperatures, current-transport only occurs when the gate

voltage V_g is tuned such that the charging energy E_{charge} become energetically degenerate for states with N and $N + 1$ electrons.

The coupling to the leads generates the additional energy scale $\Gamma = \pi \sum_\alpha \rho_\alpha(0) t_\alpha^2$, the charge fluctuation scale. t_α is the tunneling matrix element between the dot and the lead α. We can distinguish two different regimes: (i) the level spacing is large compared to the charge fluctuation scale, i. e. $\Delta\varepsilon > \Gamma$, or (ii) $\Delta\varepsilon \ll \Gamma$ which will be discussed in Sec. 4.2.

In the first case, all levels up to some level $\varepsilon_i < \varepsilon_l$ are filled and all levels $\varepsilon_i > \varepsilon_l$ are empty. The charge fluctuations just involve the spin-degenerate level $i = l$, and the Hamiltonian is identical to (14) after identifying $U = E_c$ and $\varepsilon^d = \varepsilon_l + (N_0 - N_g + \frac{1}{2})E_c$, where N_0 counts the number of occupied levels $\varepsilon_i < \varepsilon_l$. The single particle level ε^d is tuned by the external gate voltage $V_g \propto N_g$; the tunneling matrix elements take the role of the hybridization in the SIAM. In equilibrium, one can define a linear combination of both lead electrons

$$f_{0\sigma} \;=\; \frac{1}{\sqrt{t_L^2 + t_R^2}} \sum_\alpha t_\alpha c_{0\alpha\sigma} \tag{54}$$

which couples to the quantum-dot level,

$$H_T \;=\; t_0 \sum_\sigma (d_\sigma^\dagger f_{0\sigma} + f_{0\sigma}^\dagger d_\sigma) \tag{55}$$

while the orthogonal linear combination can be eliminated; $t_0 = \sqrt{t_L^2 + t_R^2}$. Hence the local dynamics is complete determined by the solution of the SIAM which contains the Kondo effect. Meir and Wingreen have shown [49] that the transmission matrix $T(z)$ governing the current transport through such a quantum dot is proportional to the local Green function of the dot, $T(z) \propto G_{\text{loc}}(z)$. At high temperatures, the transport is favored when $\varepsilon^d \approx 0$ or $\varepsilon^d + U \approx 0$. At low temperatures and $n_l \approx 1$, the Kondo effect yields a pinned maximum of the spectral function which opens up a new correlation induced transport channel: the conductance increases in the Coulomb blockade valley when lowering the temperature, which is one of the hallmarks of the Kondo-effect in SETs.

Although, this connection had been understood quite early on, the mesoscopic community believed for a long time that the exponentially smallness of the Kondo scale prevents this effect from being observed. Realizing that the Kondo resonance is adiabatically connected to the resonant-level model, David Goldhaber-Gordon was the first to see that the Kondo temperature in nano-devices can be pushed into a reasonable regime by increasing the tunneling matrix elements t_α. In a seminal paper [45], he proved the existence of the Kondo effect in a quantum dot, stimulating a huge amount of research in Kondo-related physics in nano-devices.

4.2   Charge Kondo effect

Now we discuss the opposite limit of very small level spacings, i. e. $\Delta\varepsilon \ll \Gamma$. In this regime, the levels on the quantum dot are treated as continuum, and the single-particle dynamics is modeled by two electron gases, indexed by $\alpha = L(D)$ for the single lead (states on the dot)

$$H \;=\; \sum_{k\alpha\sigma} \varepsilon_{k\alpha\sigma} c_{k\alpha\sigma}^\dagger c_{k\alpha\sigma} + \frac{t}{N} \sum_{k,q} (c_{kL\sigma}^\dagger c_{kD\sigma} + c_{kD\sigma}^\dagger c_{kL\sigma}) + E_{\text{charge}} \tag{56}$$

which are coupled by a tunneling matrix element t. To distinguish this limit from the SET, this type of quantum dot is called a quantum box since the small level spacing occurs only in devices with much larger diameters. The filling of the dot remains controlled by the charging energy E_{charge}. A fixed dot filling and, therefore, a fixed E_{charge} still enables many different configurations which share approximately the same kinetic energy. Therefore, a mapping of the electronic occupation number operator to a new charge operator $\hat{N}_c = \sum_n n|n\rangle\langle n|$ has been introduced [50]. This new operator acts on a fictitious space of charge degrees of freedom, and the mapped charging energy is given by $E_{\text{charge}} = 1/2 E_c(\hat{N}_c - N_g)^2$. Since the number of electrons in the quantum box can only change by the tunneling term, the latter requires a modification

$$H_T = \frac{t}{N} \sum_{k,q} (c_{kL\sigma}^\dagger c_{kD\sigma} + c_{kD\sigma}^\dagger c_{kL\sigma}) \;\; \rightarrow \;\; \frac{t}{N} \sum_{k,q} (c_{kL\sigma}^\dagger c_{kD\sigma} N_c^- + N_c^+ c_{kD\sigma}^\dagger c_{kL\sigma}), \quad (57)$$

where N_c^+ is the charge raising operator $\hat{N}_c^+ = \sum_n |n+1\rangle\langle n|$ and $\hat{N}_c^-$ its adjoint operator. Assigning the lead flavor up, the box flavor down, on can show that H conserves flavor, since it commutes with the flavor operator

$$\hat{N}_f \;\; = \;\; \frac{1}{2}(\hat{N}_L - \hat{N}_D) + \hat{N}_c \qquad\qquad (58)$$

where $\hat{N}_\alpha = \sum_{k\sigma} n_{k\alpha\sigma}$ account for the total number of fermions in the lead or the box.

Due to the quantization of the charge, E_{charge} can only take discrete values on a parabola with its minimum at N_g. The two lowest charge states become energetically degenerate at half-integer values of N_g. Therefore, charge fluctuations are restricted to $N, N+1$ close to $N_g = N+1/2+ \Delta n_g$ and $\beta E_c \gg 1$. With this restriction, the charging energy $E_{\text{charge}} = \frac{E_c}{2}(\frac{1}{4} - \Delta n_g \sigma_z + \Delta n_g^2)$ is converted to a Zeeman term $-E_c/2 \Delta n_g \sigma_z$, since Δn_g acts as a magnetic field in the iso-spin space of the two charge states $N, N+1$ [51]. The tunneling term H_T translates to a transversal Kondo interaction for the charge iso-spin and the physical spin, being a conserved number, converts into the conserved channel of the two-channel Kondo Hamiltonian. The effective capacitance $C(N_g, T) = -\partial\langle e\hat{N}\rangle/\partial N_g$ diverges logarithmically at $N_g = N + 1/2$ for $T \rightarrow 0$ where the prefactor $C(N_g, T) \propto -1/(T_K)\log(T/T_K)$ is governed by the two-channel Kondo scale T_K. In turned out that the NRG is the optimal tool to investigate the crossover from the classical high temperature regime to the two-channel Kondo model [52].

By coupling an additional small quantum dot to the larger quantum box as depicted in Fig. 5(b), the charging energy of the quantum box can generate a dynamical channel conservation. It has been conjectured [48] that this might be the way to experimentally realize a spin two-channel Kondo model. Interestingly, it turned out that the two-channel charge Kondo effect discussed above and the spin Kondo effect are adiabatically connected in such a complex nano-device by the two gate voltages controlling the filling in the quantum dot and the quantum box.

5   Conclusion

In this lecture, we have presented a chronological introduction to the Kondo problem. We have started with Kondo's explanation of the resistance minimum in metals weakly doped with magnetic scatterers. In the late 1960s, it was shown that Kondo's model is related to a much more general class of models, the Anderson models: Removing charge fluctuations on partially filled $3d$ and $4f$-shells, effective Kondo models can be derived using the Schrieffer-Wolff transformation.

Major progress toward a deeper understanding of the Kondo problem and its inaccessibility to perturbative approaches was made in the 1970s. In Sec. 2.1, we derived Anderson's poor man's scaling using a perturbative renormalization group approach. The first accurate solution of the problem was given by Ken Wilson in 1975 [14]. He applied his newly developed numerical renormalization group approach which elegantly circumvents the weaknesses of the perturbative treatment by using a discretized many-body Fock space. In this discrete basis, any arbitrarily complex Hamiltonian is simply defined by its matrix elements while perturbative RG approaches rely on an a-priori known low-energy field theory. We also included a discussion of exotic Kondo effects in metals where the local spin is over- or under-compensated by the coupling to conduction electron channels.

In the 1980s and 1990s, it was realized that correlated electron systems such as Heavy Fermions, High-T_c superconductors, or Mott-Hubbard are connected to the Kondo problem. In Sec. 3, we briefly introduced the dynamical mean field theory. Within DMFT, the lattice self-energy is approximated by a $\vec{k}$-independent function. Then, the complex lattice problem is mapped onto an effective impurity problem which is supplemented by the lattice self-consistency condition. This effective impurity comprises of the unit cell which is embedded in a fictitious bath of non-interaction conduction electron. Again, at the heart of its solution lies the Kondo problem: the calculation of the local self-energy requires an adequate impurity solver which remains valid for all temperature and parameter regimes of interest.

Sec. 4 has been devoted to a brief introduction of the Kondo-effect in nano-devices. We have covered two extreme limits of nano-structured quantum dots: small dots with large level spacing are used as single electron transistors. At odd fillings, the Kondo effect opens up a new transport channel which lifts the Coulomb blockade. In large dots, the level spacing is treated as continuous: the low energy physics should be governed by a two-channel Kondo model [19, 47, 48].

Acknowlegment

References

[1] J. Kondo, Prog. Theor. Phys **32**, 37 (1964)

[2] J. Kondo, J. Phys. Soc. Jpn. **74**, 1 (2005)

[3] W. de Haas, J. de Boer, and G. van den Berg, Physica **1**, 1115 (1934)

[4] A.C. Hewson, *The Kondo Problem to Heavy Fermions*
(Cambridge University Press, 1993)

[5] P.W. Anderson, Phys. Rev. **124**, 41 (1961)

[6] D.C. Langreth, Phys. Rev. **150**, 516 (1966)

[7] G. Mahan, *Many-Particle Physics* (Plenum Press, New York, 1981)

[8] J.M. Luttinger and J.C. Ward, Phys. Rev. **118**, 1417 (1960)

[9] J.R. Schrieffer and P.A. Wolff, Phys. Rev. **149**, 491 (1966)

[10] H.R. Krishna-murthy, J.W. Wilkins, and K.G. Wilson, Phys. Rev. B **21**, 1003 (1980)

[11] H.R. Krishna-murthy, J.W. Wilkins, and K.G. Wilson, Phys. Rev. B **21**, 1044 (1980)

[12] P.W. Anderson, J. Phys. C **3**, 2436 (1970)

[13] J.W. Allan and B. Mitrovic, Solid State Phys. **37**, 1 (1982),
for a review on Eliashberg theory

[14] K.G. Wilson, Rev. Mod. Phys. **47**, 773 (1975)

[15] R. Bulla, T.A. Costi, and T. Pruschke, Rev. Mod. Phys. **80**, 395 (2008)

[16] N. Andrei, K. Furuya, and J.H. Lowenstein, Rev. Mod. Phys. **55**, 331 (1983)

[17] R. Bulla, N. Tong, and M. Vojta, Phys. Rev. Lett. **91**, 170601 (2003)

[18] L.H. Yu *et al.*, Phys. Rev. Lett. **95**, 256803 (2005)

[19] D.L. Cox and A. Zawadowski, Advances in Physics **47**, 599 (1998),
for a review on the multi-channel models

[20] V.J. Emery and S. Kivelson, Phys. Rev. B **46**, 10812 (1992)

[21] D.L. Cox, Phys. Rev. Lett. **59**, 1240 (1987)

[22] C.J. Bolech and N. Andrei, Phys. Rev. Lett. **88**, 237206 (2002)

[23] F.B. Anders, Phys. Rev. B **71**, 121101 (2005)

[24] N. Grewe and F. Steglich, in *Handbook on the Physics and Chemistry of Rare Earths*, edited by K. A. Gschneidner, Jr. and L. Eyring (North-Holland, Amsterdam, 1991), Vol. 14, p. 343

[25] N. Grewe, Solid State Communications **50**, 19 (1984)

[26] Y. Kuramoto, in *Theory of Heavy Fermions and Valence Fluctuations*, edited by T. Kasuya and T. Saso (Springer, Berlin, 1985), p. 152

[27] E. Pavarini, E. Koch, D. Vollhardt, and A.I. Lichtenstein (eds.)
The LDA+DMFT approach to strongly correlated materials,
Reihe Modeling and Simulation, Vol. 1 (Forschungszentrum Jülich, 2011)
`http://www.cond-mat.de/events/correl11`

[28] N. Grewe, Z. Phys. B **67**, 323 (1987)

[29] W. Metzner and D. Vollhardt, Phys. Rev. Lett. **62**, 324 (1989)

[30] E. Müller-Hartmann, Z. Phys. B **76**, 211 (1989)

[31] U. Brandt and C. Mielsch, Z. Phys. B **75**, 365 (1989)

[32] A. Georges, G. Kotliar, W. Krauth, and M.J. Rozenberg, Rev. Mod. Phys. **68**, 13 (1996), for a review on the DMFT

[33] G. Kotliar and D. Vollhardt, Physics Today **57**, 53 (2204)

[34] K. Yamada, Prog. Theor. Phys. **54**, 316 (1975)

[35] C.D. Spataru, M.S. Hybertsen, S.G. Louie, and A.J. Millis,
Phys. Rev. B **79**, 155110 (2009)

[36] S. Schmitt and F.B. Anders, Phys. Rev. B **81**, 165106 (2010)

[37] N. Grewe, Z. Phys. B **52**, 193 (1983)

[38] Y. Kuramoto, Z. Phys. B **53**, 37 (1983)

[39] N.E. Bickers, Rev. Mod. Phys. **59**, 845 (1987)

[40] R. Peters, T. Pruschke, and F.B. Anders, Phys. Rev. B **74**, 245114 (2006)

[41] J.E. Hirsch and R.M. Fye, Phys. Rev. Lett. **56**, 2521 (1986)

[42] M. Jarrell and J.E. Gubernatis, Phys. Rep. **269**, 133 (1996),
for a review on the Maximum Entropy method

[43] E. Gull *et al.*, Rev. Mod. Phys. **83**, 349 (2011)

[44] F.B. Anders, N. Grewe, and A. Lorek, Z. Phys. B Condensed Matter **83**, 75 (1991)

[45] D. Goldhaber-Gordon *et al.*, Nature **391**, 156 (1998)

[46] M.A. Kastner, Rev. Mod. Phys. **64**, 849 (1992)

[47] K.A. Matveev, Zh. Eksp. Teor. Fiz. **99**, 1598 (1991)

[48] R.M. Potok *et al.*, Nature **446**, 167 (2007)

[49] Y. Meir and N.S. Wingreen, Phys. Rev. Lett. **68**, 2512 (1992)

[50] J. König and H. Schoeller, Phys. Rev. Lett. **81**, 3511 (1998)

[51] K.A. Matveev, Sov. Phys. JETP **72**, 892 (1991)

[52] E. Lebanon, A. Schiller, and F.B. Anders, Phys. Rev. B **68**, 041311(R) (2003)